Postprint of: Guzinski, J., Abu-Rub, H., Speed sensorless induction motor drive with motor choke and predictive control, COMPEL - The international journal for computation and mathematics in electrical and electronic engineering, Vol. 30 No. 2 (2011), pp. 686-705. DOI: 10.1108/03321641111101159

Speed sensorless induction motor drive with motor choke and predictive control

Jaroslaw Guzinski
Faculty of Electrical and Control Engineering, Gdansk University of Technology, Gdansk, Poland, and
Haitham Abu-Rub
Electrical and Computer Engineering Department, Texas A&M University at Qatar, Doha, Qatar

Abstract

Purpose
Presenting complete solution for speed sensorless AC drive with voltage source inverter, induction machine, and motor choke. Major problems with adjustable speed drives are underlined and the use of motor choke is justified. An AC drive with motor choke can work only if specific modifications in the control algorithms are done.
Design/methodology/approach
The goal of the paper is to present new nonlinear vector control method for induction motor drive. In the control system the presence of motor choke is taken into account. The choke changes the structure of the predictive controller and state observer. The new concept of integrating the predictive controller with electromagnetic forces observer is presented. The paper presents theoretical description of the system as well the simulation and experimental verification.
Findings
The paper shows that the suggested decoupled AC drive control system is operating better than system without decoupling. The system with motor choke requires modifications in the current controller and observer system. With omitting the motor choke a speed sensorless drive can not work properly.
Practical implications
The paper is closely connected with practical aspect. The solution is oriented for industrial applications because in numerous industrial dives the motor choke is utilized. However, with motor choke many sophisticated control algorithms can't work properly. The concept presented in the paper solves such practical problems.
Originality/value
The completely new are: decoupled field oriented control system with load angle controller, predictive current controller and state observer for AC drive with motor choke.

Keywords: Control systems, Electric motors, Electric converters, Filters, Observers
Paper type: Research paper

I. Introduction

Nowadays, adjustable speed drives (ASD) with induction motor (IM) and voltage inverter are commonly used in industrial systems. In more advanced drive applications with ASD and IM, the speed sensorless field oriented control (FOC) are widely implemented (Bose, 2009), (Chiasson, 2005).

The FOC principle has some variants e.g. rotor oriented, stator oriented, or others less popular (Vas, 1990). An interesting FOC scheme is the one based on control of mutual position between motor stator current and rotor flux vectors (Bogalecka, 1992). The angle between these vectors is known as the load angle or the torque angle. The good properties of such an FOC method rely on the direct influence of the angle on the generated motor torque. To improve the FOC properties, nonlinear control principles were implemented (Krzeminski, 1987), (Isidori, 1995). Even for FOC with load angle control, the nonlinear control strategy was proposed (Guzinski and Krzeminski, 2003).

An integral part of some FOC systems is the IM stator current controller. Numerous current controller methods are reported in the literature (Kazmierkowski and Malesani, 1998). Particular good properties are obtained with predictive current control (Abu-Rub H *at al.*, 2001), (Abu-Rub *at al.*, 2004), (Kouro *at al,*. 2009). The improved version of the predictive current controller with electromagnetic force observer was presented in (Abu-Rub *at al.*, 2010).

An important part of FOC systems are state variables estimators. A significant number of estimators is presented in the literature (Holtz, 2006). If the motor speed is calculated in the estimator, the drive is known as sensorless (Krzeminski, 2006). Due to economy and reliability, the sensorless solutions are readily used in the industry.

In ASD, due to high switching of power transistors, some problems are reported e.g. accelerating of the motor bearing and insulation degradation (Binder and Muetze, 2008.). To solve these negative effects, passive filters are inserted between the inverter and motor (Akagi *at al.*, 2004). Unfortunately, the filters significantly affect the structure of the system so that the sensorless ASD cannot work properly. To avoid the filter problems modification of control and estimator principles are proposed (Adamowicz and Guzinski, 2005), (Salomaki and Luomi, 2006).

The simplest version of the ASD inverter output filter is a motor choke. Motor choke reduces reflected waves in long cables connected to the motor, prevents the overvoltages on motor and inverter transistors, and reduces the radio frequency interference (RFI) level. However, in ASD with motor choke the control and estimation methods should be modified as well.

II. System Description

The presented drive with IM is supplied from voltage source inverter. The motor choke is installed on the inverter output – Fig. 1.

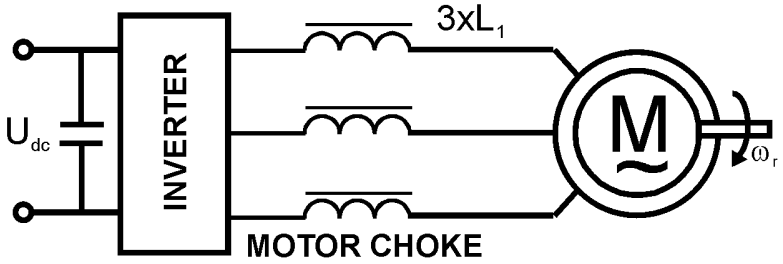

Fig. 1. Structure of AC drive with induction motor, voltage inverter and motor choke

In the proposed drive a 1.5 kW induction motor and 3.3kHz converter with IGBT transistors were used. Between the inverter and the motor three single-phase choke banks were installed. The selected parameters of the system are presented in the appendix.

The induction motor is presented as differential equations for the stator current and rotor flux vectors components. The motor model presented in per unit system (appendix) for rotating with ω_a frame of references is (Krzemiński, 1987), (Guziński and Krzeminski, 2003), (Aburub *at al.*, 2004):

$$\frac{d\mathbf{i}_s}{d\tau} = -\frac{R_s L_r^2 + R_r L_m^2}{L_r w_\sigma}\mathbf{i}_s + \frac{R_r L_m}{L_r w_\sigma}\boldsymbol{\psi}_r - j\omega_a \mathbf{i}_s - j\frac{L_m}{w_\sigma}\omega_r \boldsymbol{\psi}_r + \frac{L_r}{w_\sigma}\mathbf{u}_s \tag{1}$$

$$\frac{d\boldsymbol{\psi}_r}{d\tau} = \frac{R_r}{L_r}\boldsymbol{\psi}_r - j(\omega_a - \omega_r)\boldsymbol{\psi}_r + R_r\frac{L_m}{L_r}\mathbf{i}_s \tag{2}$$

$$\frac{d\omega_r}{d\tau} = \frac{1}{J_M}\left(\frac{L_m}{L_r}\,\mathrm{Im}\left|\boldsymbol{\psi}_r^* \mathbf{i}_s\right| - T_L\right) \tag{3}$$

where: ω_r – is motor mechanical speed, $\mathbf{i}_s=[i_{s\alpha}\ i_{s\beta}]^T$ is stator current vector, $\mathbf{u}_s=[u_{s\alpha}\ u_{s\beta}]^T$ is stator voltage vector, $\boldsymbol{\psi}_s=[\psi_{r\alpha}\ \psi_{r\beta}]^T$ is rotor flux vector, τ is time in per unit system, R_r, R_s, L_r, L_s, L_m are motor parameters, T_L is load torque, J_M is motor inertia and:

$$w_\sigma = L_r L_s - L_m^2 \tag{4}$$

The motor choke is described by:

$$\frac{d\mathbf{i}_s}{d\tau} = \frac{1}{L_1}(\mathbf{u}_1 - \mathbf{u}_s) \tag{5}$$

where: $\mathbf{u}_1=[u_{s\alpha}\ u_{s\beta}]^T$ is inverter output voltage vector, L_1 is motor choke inductance.

In the investigated drive system with induction motor, voltage inverter, and motor choke the voltage and current waveforms are as shown in Fig. 2.

a)

b)

c)

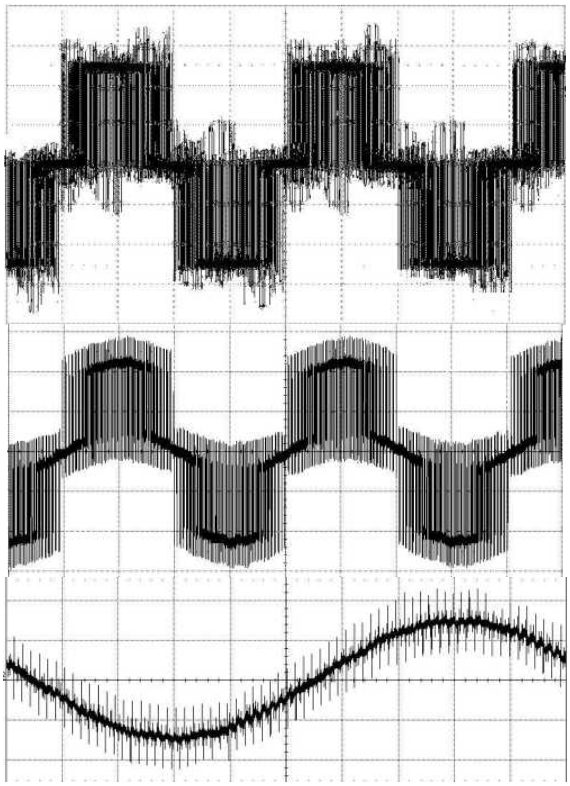

Fig. 2. Waveforms in the drive with induction motor, inverter and motor choke: a) inverter output voltage, b) motor supply voltage, c) motor current (a, b – 200 V/div, 5ms/div; c – 5A/div, 2ms/div) – recorded waveforms are not time synchronised

The waveforms in Fig 2 were obtained for loaded motor; the motor current was equal to 5A. With a motor choke the motor supply voltage pulse rate-of-rise (dv/dt) is limited – Fig. 3.

a)

b)

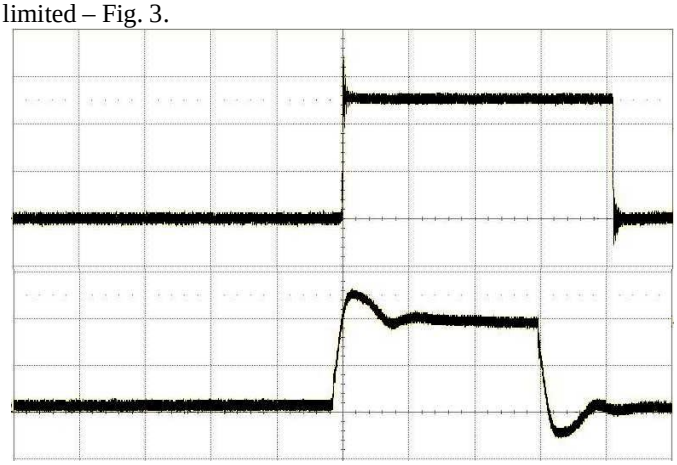

Fig. 3. Waveforms in the drive with induction motor, inverter, and motor choke: a) voltage wave on choke input, b) voltage wave on choke output (10μs/div, 200V/div) – recorded waveforms are not time synchronised

It is noticeable in Fig. 3 that the motor supply voltage rate of rise (dv/dt) is limited in relation to inverter output voltage.

III. Control System

Among different control algorithms the control of the load angle FOC control exists (Bogalecka, 1992) The structure of the load angle control seems are simpler in contrary to the FOC because they don't need Park transformations. The load angle δ is noted as an angle between the $\boldsymbol{\psi}_r$ and $\mathbf{i}_s$ vectors. Controlling of that vector amplitudes and mutual position gives the possibility to control the motor electromagnetic torque T_e:

$$T_e = k \cdot \mathrm{Im}\left(\boldsymbol{\psi}_r^* \mathbf{i}_s\right) = k\left|\boldsymbol{\psi}_r\right|\left|\mathbf{i}_s\right| \sin\delta \tag{6}$$

where: k - constant of proportionality.

The FOC load angle control system base structure based on (5) is presented in Fig. 4.

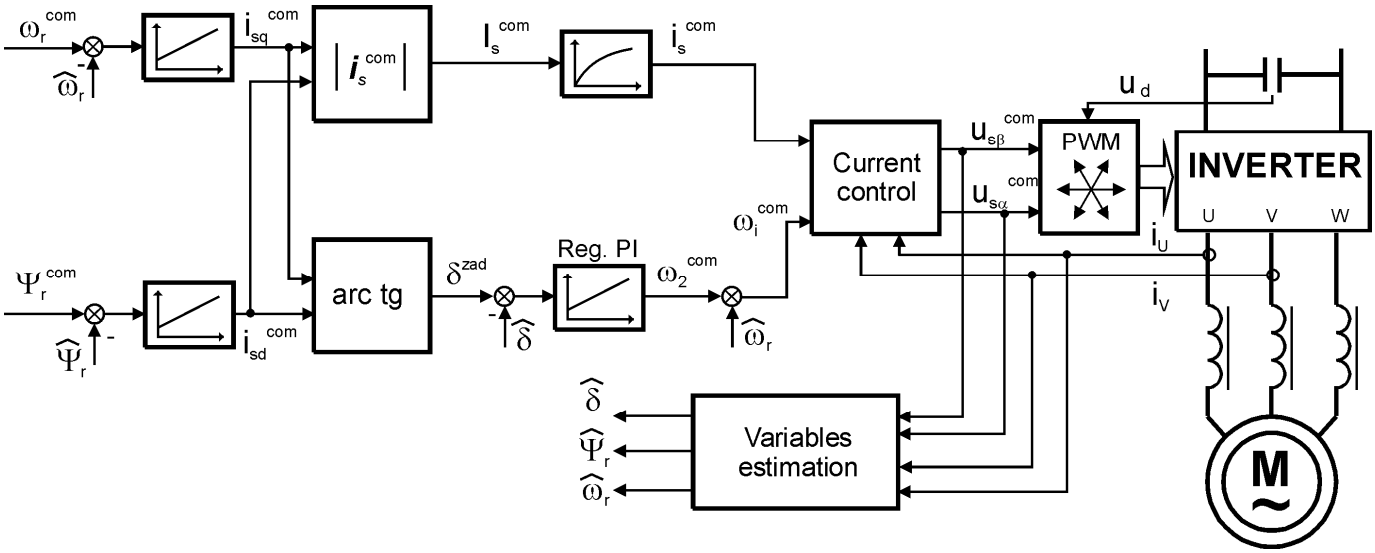

Fig. 4. Base structure of the FOC algorithm with load angle control (^ denotes variables evaluated in estimation block)

In the control system in Fig. 4 the measured variables are inverter output currents and inverter DC link voltage. The motor currents and motor voltages are not measured. The load angle is controlled by commanding the motor slip frequency ω_2. The sum of ω_2 and motor speed ω_r is noted as current commanded angular frequency ω_i^{com}. The signal ω_i^{com} simultaneously with commanded stator current magnitude i_s^{com} are controlled by the current controller algorithm. The current controller cooperates with pulse width modulation (PWM) procedure. The commanded values of I_s and ω_i are set by speed and flux module controllers with the output signals I_s^{com} and δ^{com}:

$$I_s^{com} = \sqrt{\left(i_{sd}^{com}\right)^2 + \left(i_{sq}^{com}\right)^2} \tag{7}$$

$$\delta^{com} = \mathrm{arc\,tg}\left(\frac{i_{sq}^{com}}{i_{sd}^{com}}\right) \tag{8}$$

The amplitudes of $\boldsymbol{\psi}_r$ and $\mathbf{i}_s$ vectors are kept constant while the motor torque is controlled by changing the angle δ. Unfortunately, in transients some coupling and interactions appear between the controlled variables. This is due to inherent nonlinearities and couplings existing in the induction motor.

To eliminate these negative features appearing in the drive the nonlinear control principles (Isidori, 1995) were implemented – e.g. as in (Krzeminski, 1987).

The nonlinear control principle is implemented for the FOC system presented in Fig. 4. The linearization and decoupling of the Fig. 4 structure is based on equations of the current controlled induction motor model described by the next dependencies:

$$\frac{di_s}{d\tau} = \frac{1}{T_i}\left(i_s - I_s^{com}\right) \tag{9}$$

$$\frac{d\delta}{d\tau} = -\frac{R_r L_m}{L_r}\frac{i_s}{\psi_r} + \omega_i - \omega_r \tag{10}$$

$$\frac{d\psi_r}{d\tau} = -\frac{R_r}{L_r}\psi_r + \frac{R_r L_m}{L_r} i_s \cos\delta \tag{11}$$

$$\frac{d\omega_r}{d\tau} = -\frac{1}{J_M}\left(\frac{L_m}{L_r}\psi_r i_s - T_L\right) \tag{12}$$

where: i_s, u_s are stator current and voltage modules, ψ_r is rotor flux module, I_s^{com} is commanded stator current, and T_i is time constant of the low pass filter (LPF) related to the inertia of elements appearing in current control loop.

Equation (9) exists only in the control system and is added to model the physical limitation of the stator current pulsation changes.

Based on the analysis of (10) and (11), the linearization and decoupling of the systems is performed. To assure system stability, the relationship of cos δ in (11) should be positive. Otherwise, positive feedback can appear in the control loop. To assure cos δ>0 the angle δ is limited to (-π/2.. π/2) range and then new control variable ψ_r^* is introduced:

$$\psi_r^* = L_m i_s \cos\delta\,, \tag{13}$$

From (13) the commanded stator current module is calculated:

$$i_s^{com} = \frac{\psi_r^*}{L_m \cos\delta} \tag{14}$$

The LPF equation (8) is replaced by LPF dependency for rotor flux magnitude:

$$\frac{d\psi_{ri}^*}{dt} = \frac{1}{T_\psi}\left(\psi_{ri}^* - \psi_r^*\right) \tag{15}$$

where ψ_{ri}^* is an output signal of LPF and T_ψ is LPF inertia.

According to (15) the equation (14) has the form:

$$i_s^{com} = \frac{\psi_{ri}^*}{L_m \cos\delta} \tag{16}$$

If the control signal (13) is substituted in (10), then the dynamic of load angle is transformed into the form:

$$\frac{d\delta}{d\tau} = -\frac{R_r}{L_r}\frac{\psi_{ri}^*}{\psi_r \cos\delta} + \omega_i - \omega_r \tag{17}$$

which is still nonlinear. To transform (17) into a linear form, the commanded motor current pulsation should be:

$$\omega_i^{com} = \omega_r + \frac{R_r}{L_r}\frac{\psi_r^*}{\psi_r \cos\delta} + \frac{1}{T_\delta}\left(\delta^* - \delta\right) \tag{18}$$

where δ^* and T_δ are desired load angle and time constant of the load angle dynamic system respectively.

With regard to (18) and (13), the next dynamic system for load angle and rotor flux control is obtained:

$$\frac{d\delta}{d\tau} = \frac{1}{T_\delta}\left(\delta^* - \delta\right) \tag{19}$$

$$\frac{d\psi_r}{d\tau} = \frac{R_r}{L_r}\left(\psi_{ri}^* - \psi_r\right) \tag{20}$$

It is noticeable that the dynamic system (19)-(20) is linear and decoupled.

The structure of the nonlinear FOC with load angle controller is presented in Fig. 5.

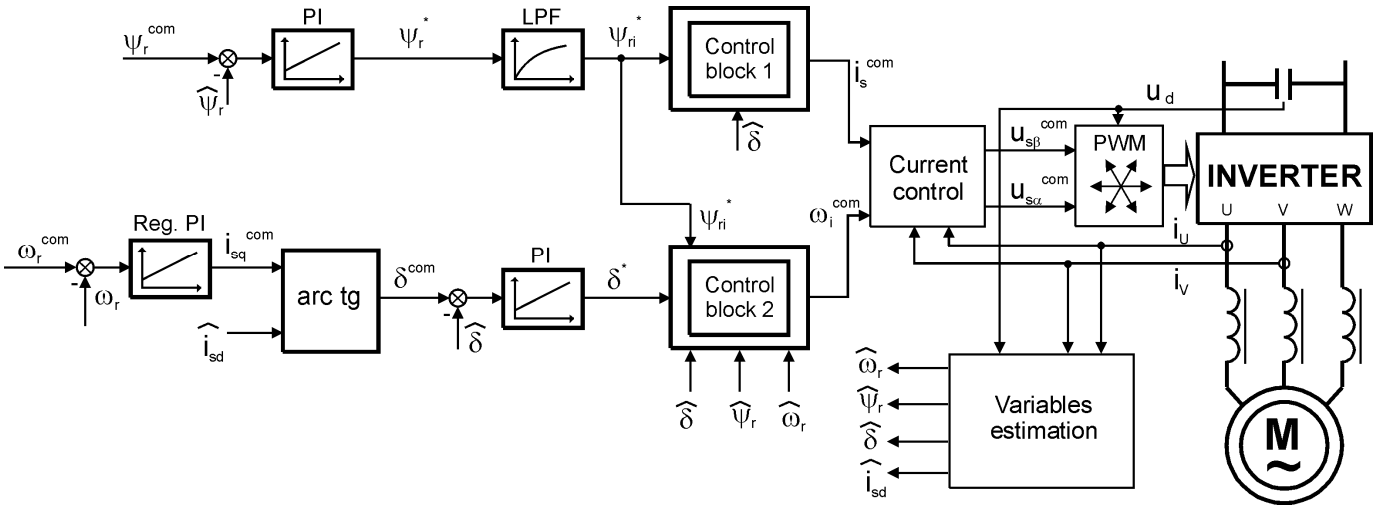

Fig. 5. Structure of the nonlinear FOC with load angle control

In the system from Fig. 5 the commanded value of load angle is:

$$\delta^{com} = \text{arc tg}\left(\frac{i_{sq}^{com}}{\hat{i}_{sd}}\right) \tag{21}$$

The commanded stator current amplitude is calculated in control block 1 based on (16) and the commanded stator current pulsation is calculated in control block 2 based on equation (18). Both blocks are indicated in Fig. 5.

IV. Predictive Current Controller

In the presented control system the motor stator current is controlled. For that purpose the predictive current controller was implemented. The predictive current controller uses actual values of the induction motor electromagnetic forces **e** (EMF) to obtain proper current regulation. Values of the EMF are calculated in the observer system described in the next chapter.

The notation for the presented current controller is explained in Fig. 6.

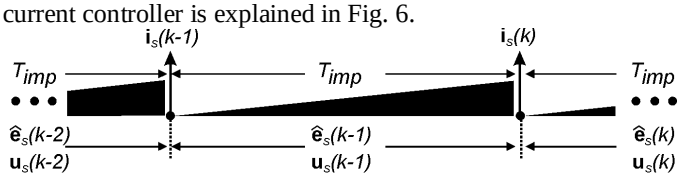

Fig. 6. Samples notation for switching period *Timp*

The basic assumption is that the PWM inverter is working in such a way that inverter output voltage $\mathbf{u}_s$ is equal to its commanded value $\mathbf{u}_s^{com}$:

$$\mathbf{u}_s \approx \mathbf{u}_s^{com} \tag{22}$$

The current controller principle is based on the dynamic equation that describes the model of the system. An equivalent model of the presented system contains three parts: inductance, resistance, and EMF. Because a motor choke is installed in the ASD, it is acceptable to neglect an equivalent resistance of the load. With such assumption the system dynamic is described:

$$\frac{d\mathbf{i}_s}{d\tau} = \frac{1}{L_1 + L_\sigma}\left(\mathbf{u}_s^{com} - \mathbf{e}\right) \tag{23}$$

where $\mathbf{u}_s^{com}$ is inverter commanded voltage vector and T_{imp} is inverter switching frequency period.

For small T_{imp} the equation (23) is approximated as follow:

$$\frac{\mathbf{i}_s(k) - \mathbf{i}_s(k-1)}{T_{imp}} = \frac{1}{L_1 + L_\sigma}\left(\mathbf{u}_s^{com}(k-1) - \mathbf{e}(k-1)\right) \tag{24}$$

If (k-1)..(k) time period is taken into account the variables $\mathbf{i}_s(k)$ and $\mathbf{e}(k-1)$ are unknown and should be predicted on base of previous known samples.

In the presented system EMF is calculated on-line in the estimation block:

$$\hat{\mathbf{e}} = \omega_r \hat{\boldsymbol{\psi}}_r \tag{25}$$

Motor EMF (25) is calculated inside an observer structure presented in the next section.

The samples of $\hat{\mathbf{e}}(k-2)$ and $\hat{\mathbf{e}}(k-3)$ calculated in the observer are memorized and used to predict value of $\hat{\mathbf{e}}(k-1)$:

$$\hat{\mathbf{e}}^{pred}(k-1) = \mathbf{C}_{EMF}\hat{\mathbf{e}}(k-2) \tag{26}$$

where

$$\mathbf{C}_{EMF} = \begin{bmatrix} \cos(\Delta\varphi_e) & \sin(\Delta\varphi_e) \\ -\sin(\Delta\varphi_e) & \cos(\Delta\varphi_e) \end{bmatrix} \tag{27}$$

and $\Delta\varphi_e$ is **e** vector angular position change:

$$\Delta\varphi_e = a\tan\frac{\hat{e}_\alpha(k-2)\hat{e}_\beta(k-3) - \hat{e}_\alpha(k-3)\hat{e}_\beta(k-3)}{\hat{e}_\alpha(k-2)\hat{e}_\alpha(k-3) + \hat{e}_\beta(k-2)\hat{e}_\beta(k-3)} \tag{28}$$

For calculated $\hat{\mathbf{e}}^{pred}$ value the current sample at (k) is predicted:

$$\mathbf{i}_s^{pred}(k) = \mathbf{i}_s(k-1) + \frac{T_{imp}}{L_1 + L_\sigma}\left(\mathbf{u}_s^{com}(k-1) - \hat{\mathbf{e}}^{pred}(k-1)\right) \tag{29}$$

The current regulation errors at instant (k-1) and (k) are calculated as follows:

$$\Delta\mathbf{i}_s(k-1) = \mathbf{i}_s^{com}(k-1) - \mathbf{i}_s(k-1) \tag{30}$$

$$\Delta\mathbf{i}_s(k) = \mathbf{i}_s^{com}(k) - \mathbf{i}_s^{pred}(k) \tag{31}$$

In order to minimize stator current regulation error at (k+1) instant the proper voltage vector $\mathbf{u}_s^{com}(k)$ should be applied (Aburub *et al.*, 2010):

$$\mathbf{u}_s^{com}(k) = \frac{L_1 + L_\sigma}{T_{imp}}\left(\mathbf{i}_s^{com}(k+1) - \mathbf{i}_s^{pred}(k) + \mathbf{D}_{Is}\right) + \hat{\mathbf{e}}^{pred}(k) \tag{32}$$

where $\mathbf{D}_{Is}$ is current controller correction feedback:

$$\mathbf{D}_{Is} = W_1\mathbf{C}_{EMF}\Delta\mathbf{i}_s(k) + W_2\mathbf{C}_{2EMF}\Delta\mathbf{i}_s(k-1) \tag{33}$$

and:

$$\hat{\mathbf{e}}^{pred}(k) = \mathbf{C}_{2EMF}\hat{\mathbf{e}}(k-2) \tag{34}$$

$$\mathbf{C}_{2EMF} = \begin{bmatrix} \cos(2\Delta\varphi_e) & \sin(2\Delta\varphi_e) \\ -\sin(2\Delta\varphi_e) & \cos(2\Delta\varphi_e) \end{bmatrix} \tag{35}$$

In (33) W_1 and W_2 are tuned parameters (Abur-Rub *at al.*, 2010), (Wojciechowski and Krzeinski, 2001)

The predictive current controller structure is presented in Fig. 7.

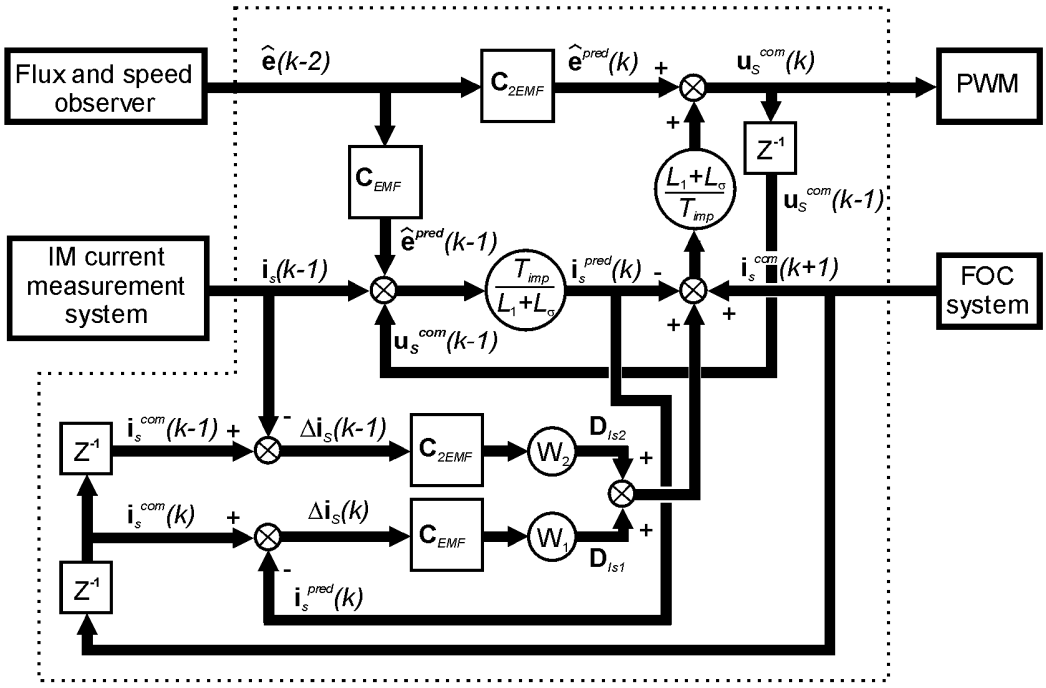

Fig. 7. Predictive current controller structure for ASD with motor choke

An important parameter of the system is the inductance, which appears in the current controller relationships. Therefore, it is indispensable to add the motor choke inductance L_1 to the current controller equations.

V. Variables Estimation Technique

Properties of the FOC are strictly dependent on the used estimation technique. Therefore, a lot of research is dedicated to that subject (Rajashekara *et al.*, 1995), (Krzeminski 2000), (Holtz, 2006). Only few of the work efforts give attention to the ASD, in which filters are installed between motor and inverter (Adamowicz and Guzinski, 2005), (Salomaki and Luomi, 2006), (Guzinski, 2008), (Guzinski, 2009).

In case of ASD with motor filters, or simply the motor choke, the choke parameters should be taken into account in the estimation procedure.

In this paper the disturbance observer (Krzeminski, 2000) is implemented taking into account the motor choke presence. In the observer, the motor EMF is treated as disturbance with components in αβ coordinates calculated using exact disturbance model (Krzeminski, 2008):

$$\frac{d\boldsymbol{\xi}}{d\tau} = \frac{R_r}{L_r}\boldsymbol{\xi} + R_r \frac{L_m}{L_r}\omega_r \mathbf{i}_s + j\hat{\omega}_r\boldsymbol{\xi} \tag{36}$$

where :

$$\xi_\alpha = \psi_{r\alpha}\omega_r \tag{37}$$

$$\xi_\beta = \psi_{r\beta}\omega_r \tag{38}$$

$$\boldsymbol{\xi} = \begin{bmatrix}\xi_\alpha & \xi_\beta\end{bmatrix}^T \tag{39}$$

In case of the ASD with motor choke the disturbance observer is modified similarly to solution presented in (Guzinski, 2009). In case of ASD with motor choke the L_1 inductance is added to the motor model – Fig. 8.

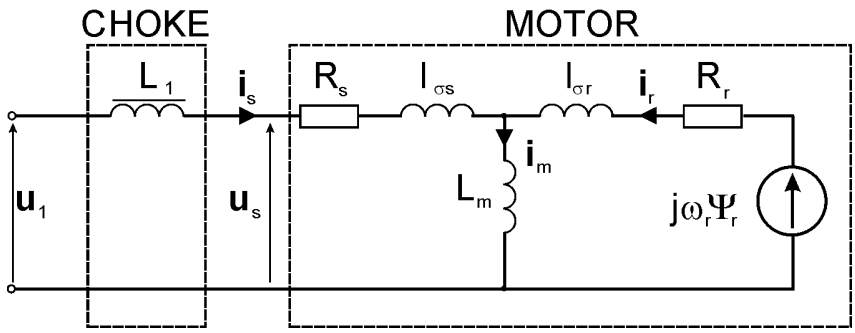

Fig. 8. Induction motor drive with voltage inverter and motor choke

The equations of the proposed observer for ASD with motor choke are follows:

$$\frac{d\hat{\mathbf{i}}_s}{d\tau} = -\frac{R_s L_r^2 + R_r L_m^2}{L_r w_{\sigma 1}}\hat{\mathbf{i}}_s + \frac{R_r L_m}{L_r w_{\sigma 1}}\hat{\boldsymbol{\psi}}_r - j\frac{L_m}{w_{\sigma 1}}\hat{\boldsymbol{\xi}} + \frac{L_r}{w_{\sigma 1}}\mathbf{u}_1^{com} + k_1\left(\mathbf{i}_s - \hat{\mathbf{i}}_s\right) \tag{40}$$

$$\frac{d\hat{\boldsymbol{\psi}}_r}{d\tau} = \frac{R_r}{L_r}\hat{\boldsymbol{\psi}}_r + R_r\frac{L_m}{L_r}\hat{\mathbf{i}}_s + j\hat{\boldsymbol{\xi}} + \mathbf{e}_\psi \tag{41}$$

$$\frac{d\hat{\boldsymbol{\xi}}}{d\tau} = \frac{R_r}{L_r}\hat{\boldsymbol{\xi}} + R_r\frac{L_m}{L_r}\omega_r\hat{\mathbf{i}}_s + j\hat{\omega}_r\hat{\boldsymbol{\xi}} + jk_4\left(\mathbf{i}_s - \hat{\mathbf{i}}_s\right) \tag{42}$$

$$\frac{dS_{bF}}{d\tau} = k_{fo}\left(S_b - S_{bF}\right) \tag{43}$$

where: $\mathbf{e}_\psi = \left[-k_2 S_b\hat{\psi}_{r\alpha} + k_3\hat{\psi}_{r\beta}\left(S_b - S_{bF}\right) \quad -k_2 S_b\hat{\psi}_{r\beta} - k_3\hat{\psi}_{r\alpha}\left(S_b - S_{bF}\right)\right]^T$, k_1, k_2 and k_4 are observer gains, S_b is observer stabilizing component, S_{bF} is S_b filtered value and:

$$w_{\sigma 1} = L_r\left(L_s + L_1\right) - L_m^2 \tag{44}$$

The rotor mechanical speed is estimated as follows (Krzeminski, 2008):

$$\hat{\omega}_r = \frac{\hat{\xi}_\alpha\hat{\psi}_{r\alpha} + \hat{\xi}_\beta\hat{\psi}_{r\beta}}{\Psi_r^2} \tag{45}$$

In (40)-(43) due to assuming a small step of the observer calculation, the derivative of estimated speed was neglected.

For the current predictive controller the value of motor EMF **e** is equal to ξ calculated in (42).

VI. Simulation Investigations

In the first step, the presented drive was investigated in simulation using a special software prepared in C language.

Fig. 9 presents the operation of the drive without the FOC loop; only with current controller. The current controller operates correctly with current regulation error less then 5%. At the 100ms instant, the current algorithm was changed – the inductance of the motor choke L_1 was equated to zero. It is noticeable that due to huge regulation error, an ASD can't work correctly if the choke parameters are not taken into account.

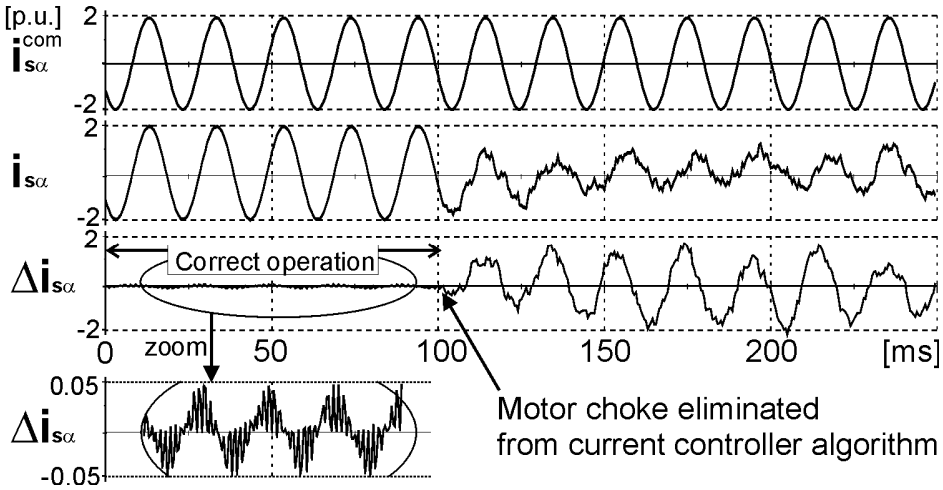

Fig. 9. Current controller operation - at instant 100ms the motor choke L_1 was eliminated from current controller equations

Fig. 10 presents an operation of the full control system without nonlinear feedback. The structure of the system is based on scheme presented in Fig. 4. In steady state, the system controls correctly the commanded speed and flux, but in transients the interaction between both regulation systems appear. In case of speed reverse a huge flux error appears. In the real system the drive operating without the decoupled control will not work in a stable manner. The stable work of this system is possible only when ASD dynamic is limited. In the real system, flux will be limited due to magnetic circuit saturation. This was not observed in the simulation because a linear model of the motor was assumed.

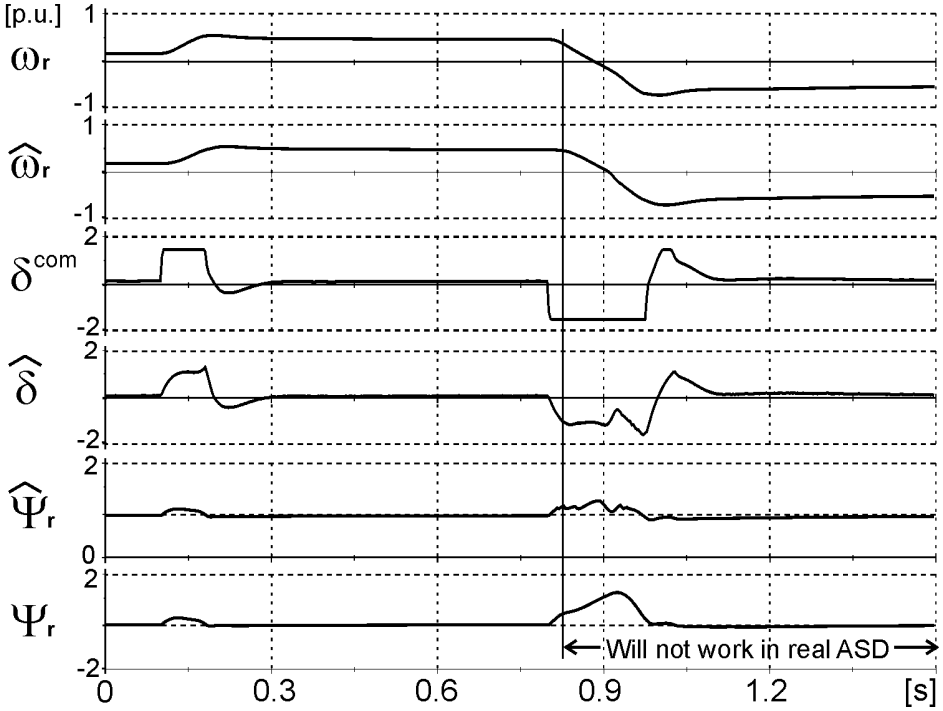

Fig. 10. The speed sensorless induction motor control in case of the speed variation in the control system without linearization feedback – the control structure is as presented in Fig. 4

In Fig. 11-Fig 14 the operation in speed sensorless nonlinear FOC system with load angle controller are presented.

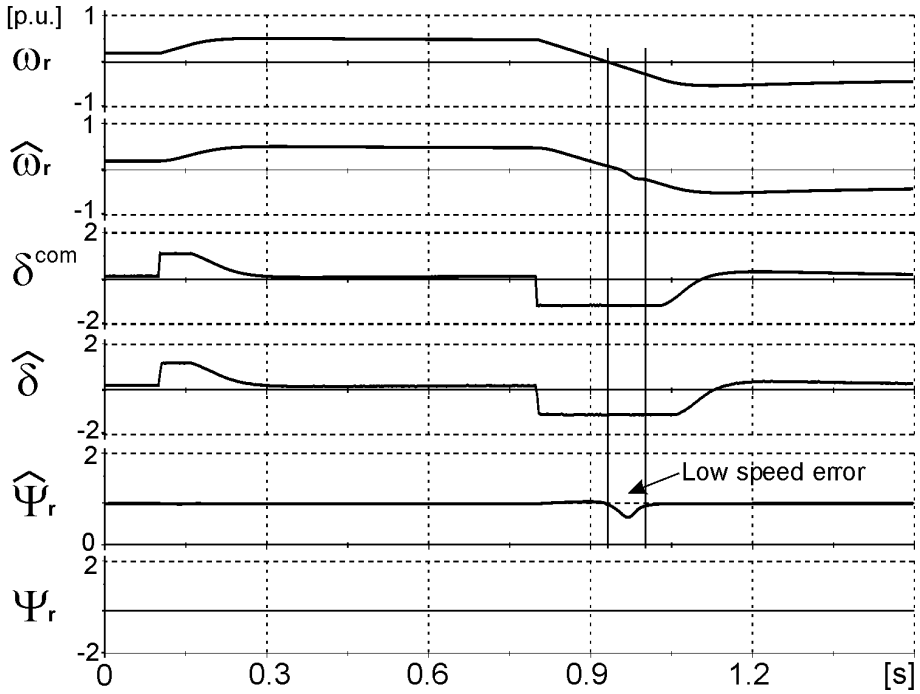

Fig. 11. The speed sensorless induction motor control in case of the speed variation in the control system **with linearization feedback** for speed variations– the control structure is as presented in Fig. 5

In Fig. 11 the commanded speed variations are done with speed reverse. In comparison with Fig. 9a better properties are observed. The decrease of the motor speed at 0.1s has no influence on motor flux. The estimated load angle is the same as the commanded value. Only for speed reverse the calculated flux is decreased whereas the real flux is kept constant. It is the result of passing the observer through unstable point which typically appears in the low speed regenerative mode. Such phenomenon is typical for induction motor observers (Kubota *et al.*, 2002). Fortunately, the phenomenon has negligible influence on system work.

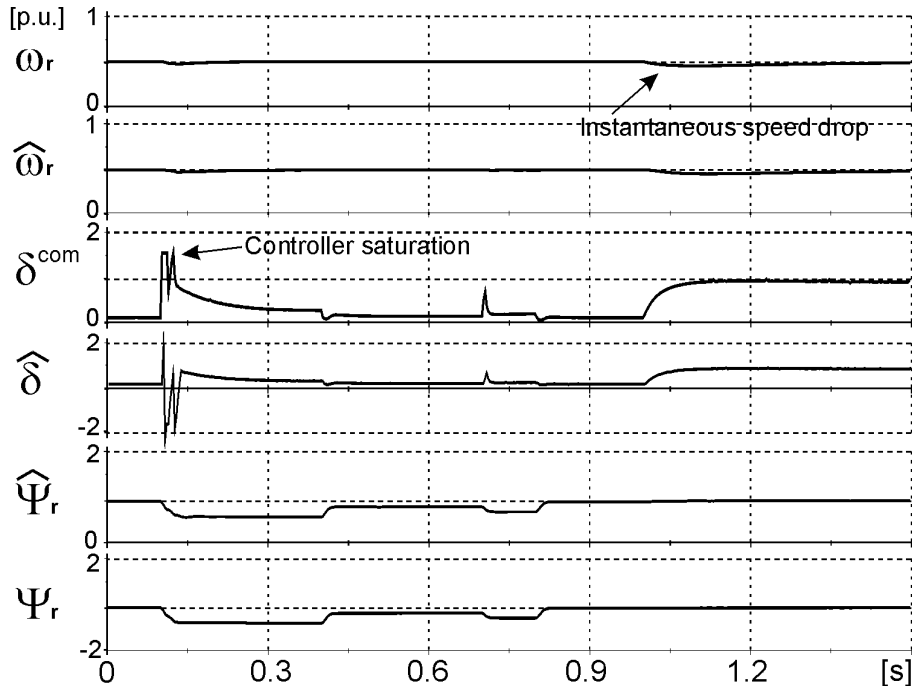

Fig. 12. Speed variation for the sensorless control system **with linearization feedback** with flux and load torque variations– control structure as is in Fig. 5

In Fig. 12 operation of the ASD under flux and load torque variations is presented. The flux variations have no influence on speed control loop except at the moments where controller saturation occurs. Under step change of load torque at 1s, instant small speed drop appears until it is compensated by speed controller at 1.3s instant.

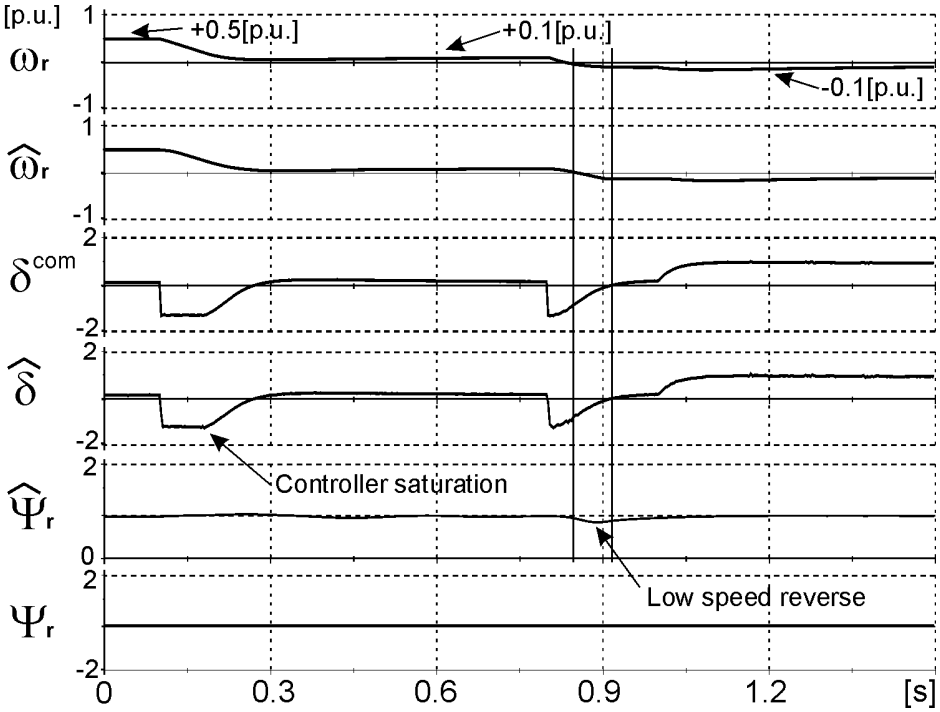

Fig. 13. Speed variation for the sensorless control system **with linearization feedback** and low speed variations– control structure from Fig. 5

In Fig. 13, the ASD operation under speed variations, including low speed ranges, is presented. The system correctly keeps the commanded speed and flux. Interactions between torque and flux regulations result from the controller's saturation during passing the regenerative mode during speed reverse.

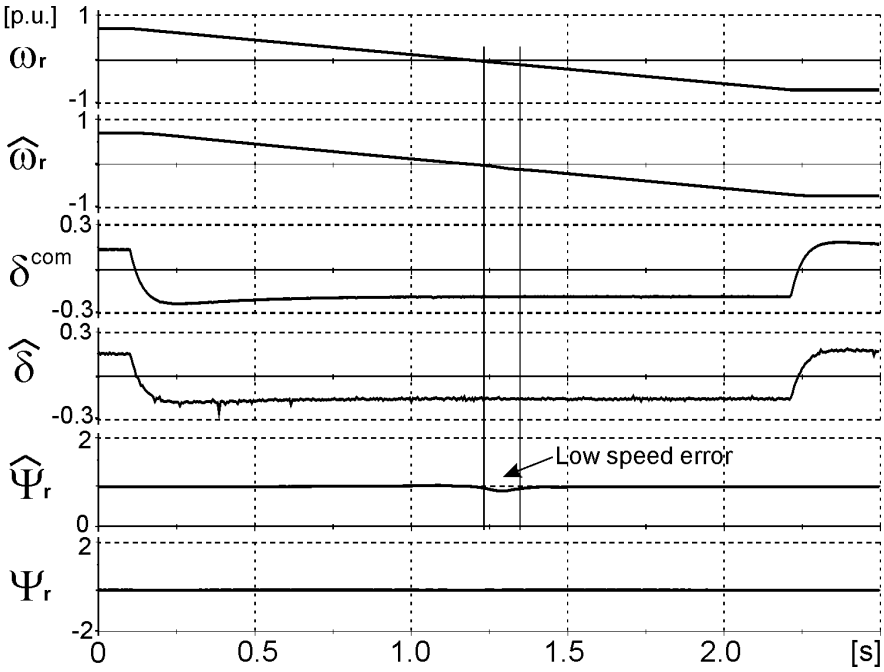

Fig. 14. Speed variation in the sensorless control system **with linearization feedback** for slow speed reverse– the control structure is based as is in Fig. 5

A slow reverse of the proposed ASD with feedback linearization is presented in Fig. 14. In comparison with previous fast speed reverse, the estimated flux, which appears during passing through regenerative mode, is smaller. The whole system works properly.

VII. Experimental Results

The experimental setup consists of a 1.5 kW induction motor drive system with data presented in appendix.

In the experimental system, an induction motor was fed by voltage source inverter controlled by DSP board SH65L type – Fig 15. In SH65L board ADSP21065L floating point digital signal processor (DSP) and the field programmable gate array (FPGA) were used. The SH65L board was connected to the PC computer where the control software was installed. In the PWM, the simple compensation of the dead time effects was implemented. For control purposes, one DC voltage and two current sensors were installed in the system. Only for data acquisition purposes the motor speed sensor was used. To set the induction motor load torque, a separately excited dc generator with controlled rectifier was used.

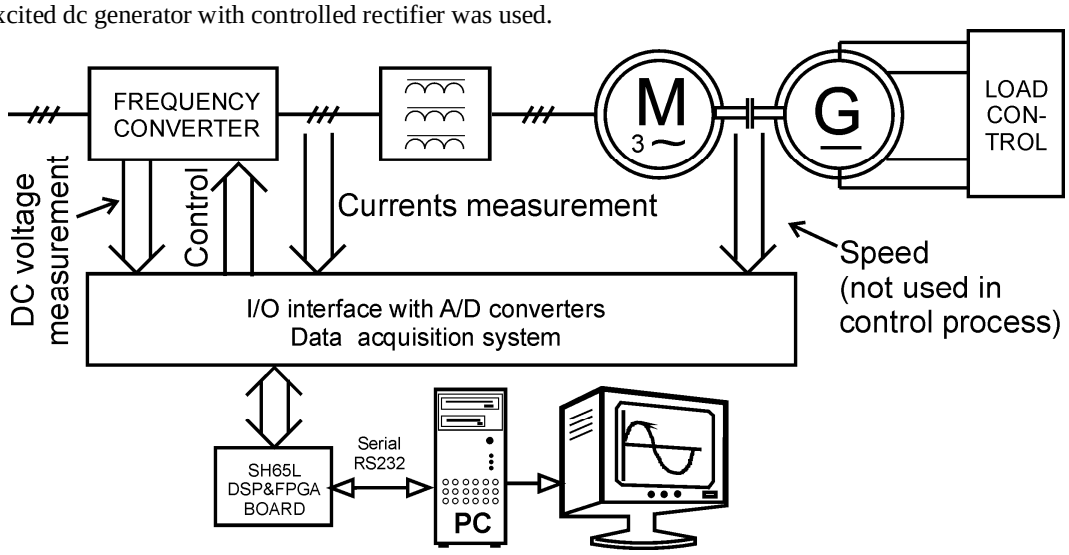

Fig. 15. Experimental test bench

Experimental results are presented in Fig. 16 – Fig. 19

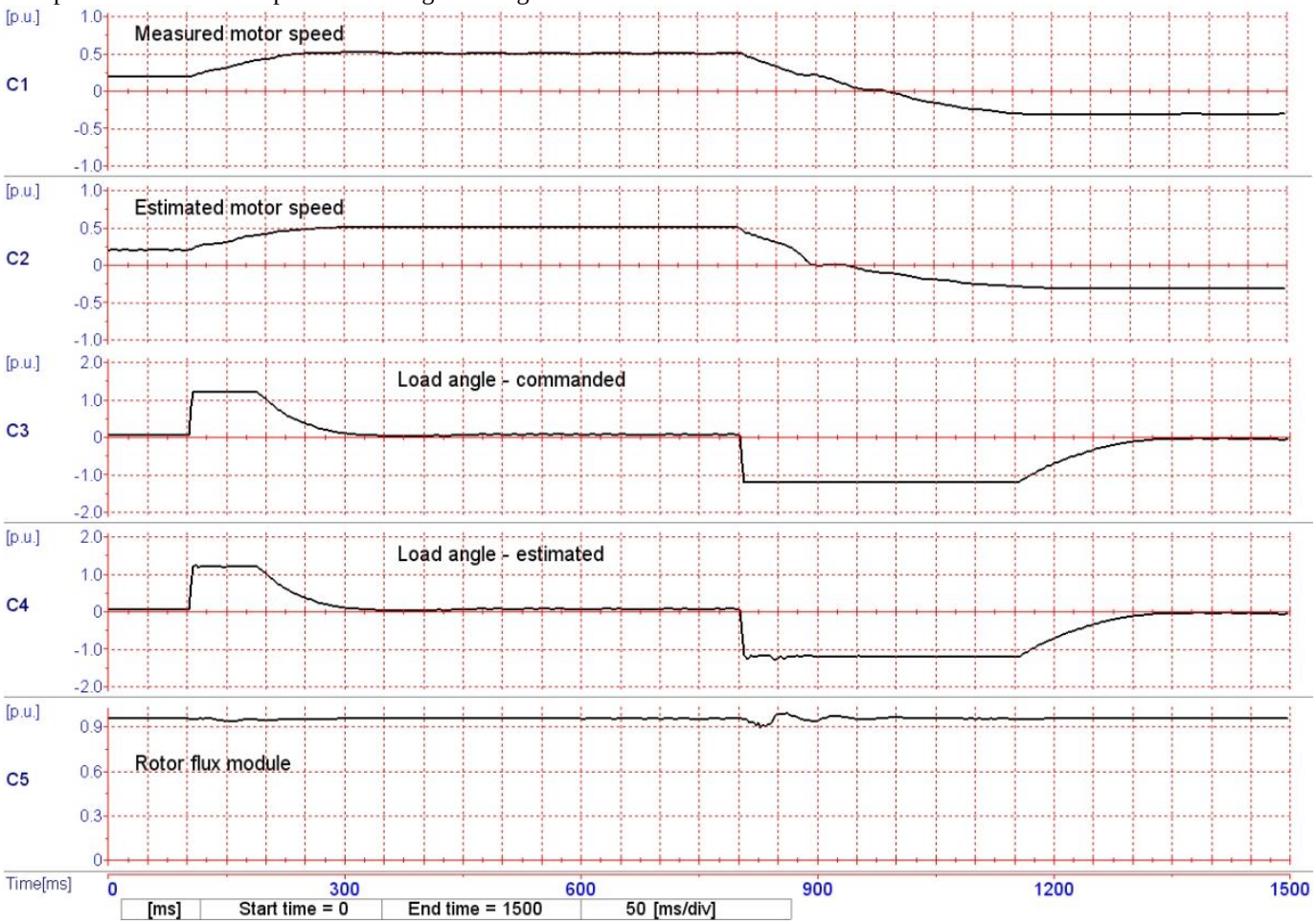

Fig. 16. The speed sensorless induction motor control results in case of the speed variation (Channels: C1-ω_r, C2-$\hat{\omega}_r$, C3-δ^{com}, C3-$\hat{\delta}$, C5-$\left|\hat{\Psi}\right|_r$)

In Fig. 16 test, the commanded motor speed was changed: increased and decreased with speed reverse. The speed controller was designed for the fastest possible action without overshoot. As a result of high dynamics of the tested ASD, small oscillations in the flux are observed during very fast motor torque changes. It is a result of the controllers' saturation, which disturbs the decoupling structure of the drive. The estimated speed has some error in the lower region as was reported in (Krzeminski, 2000), (Rajashekara, 1995) and (Krzeminski 2002). In spite of such errors, the whole system maintains robustness and stability.

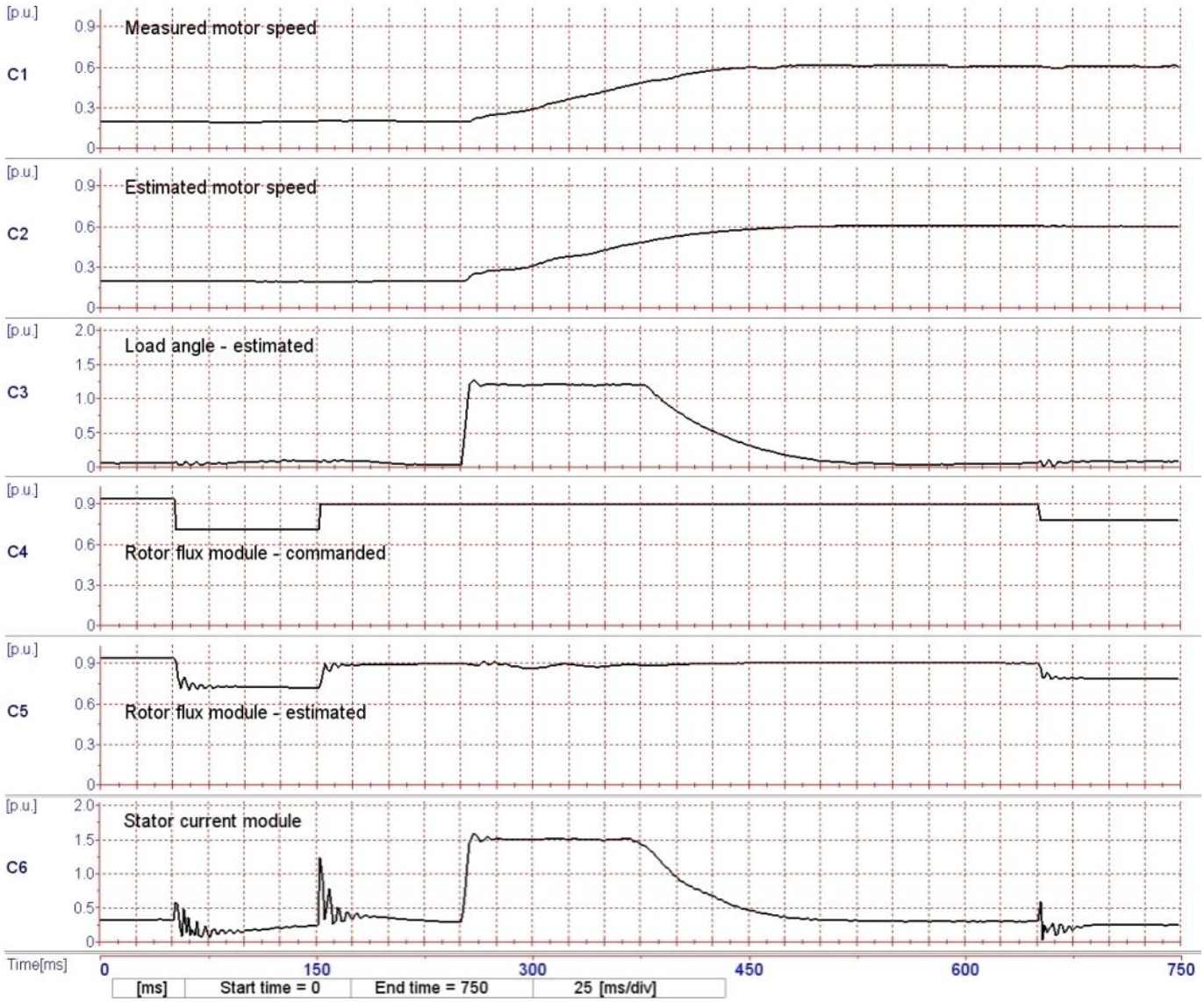

Fig. 17. The speed sensorless induction motor control results in case of the commanded flux and speed variation (Channels: C1-ω_r, C2-$\hat{\omega}_r$, C3-$\hat{\delta}$, C4-Ψ_r^{com}, C5-$\left|\hat{\Psi}\right|_r$, C6-$i_s$)

In Fig. 17 both commanded flux and motor speed were changed. The flux and motor speed follow their commanded values. Tested system of the ASD with motor choke operates correctly.

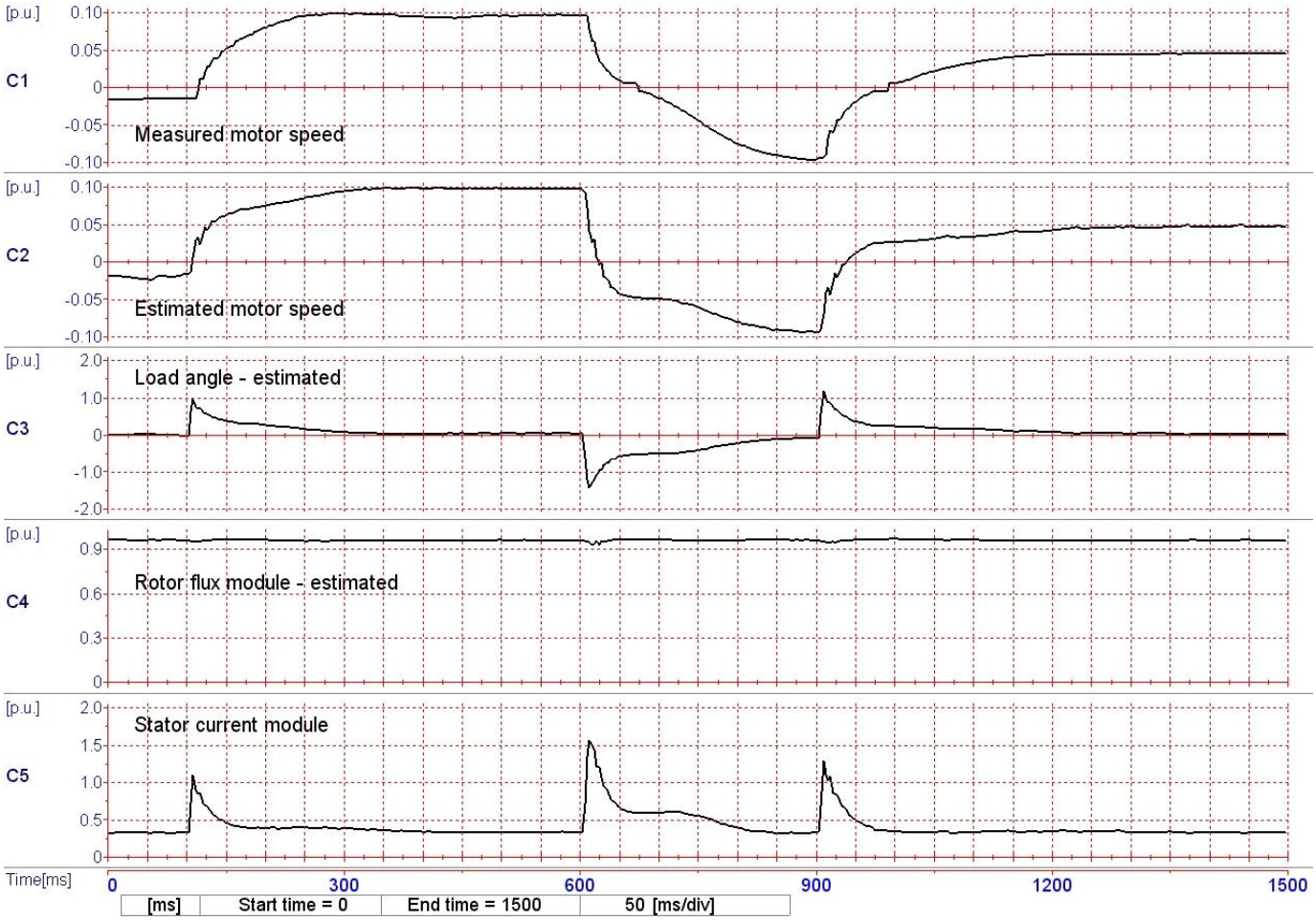

Fig. 18. The speed sensorless induction motor control in case of the low speed variation
(Channels: C1-ω_r, C2-$\hat{\omega}_r$, C3-$\hat{\delta}$, C4-$|\Psi|_r$, C5-i_s)

Low speed tests are presented in Fig. 18. The speed estimation error appears at the beginning part of the reverse process. That phenomenon was observed in previous experiments and simulations. This was also reported in (Rajashekara, 1995), where special attention was given to lower speed operation including the regenerative region. The proposed ASD is robust for such errors while the whole system keeps stability with nearly constant flux.

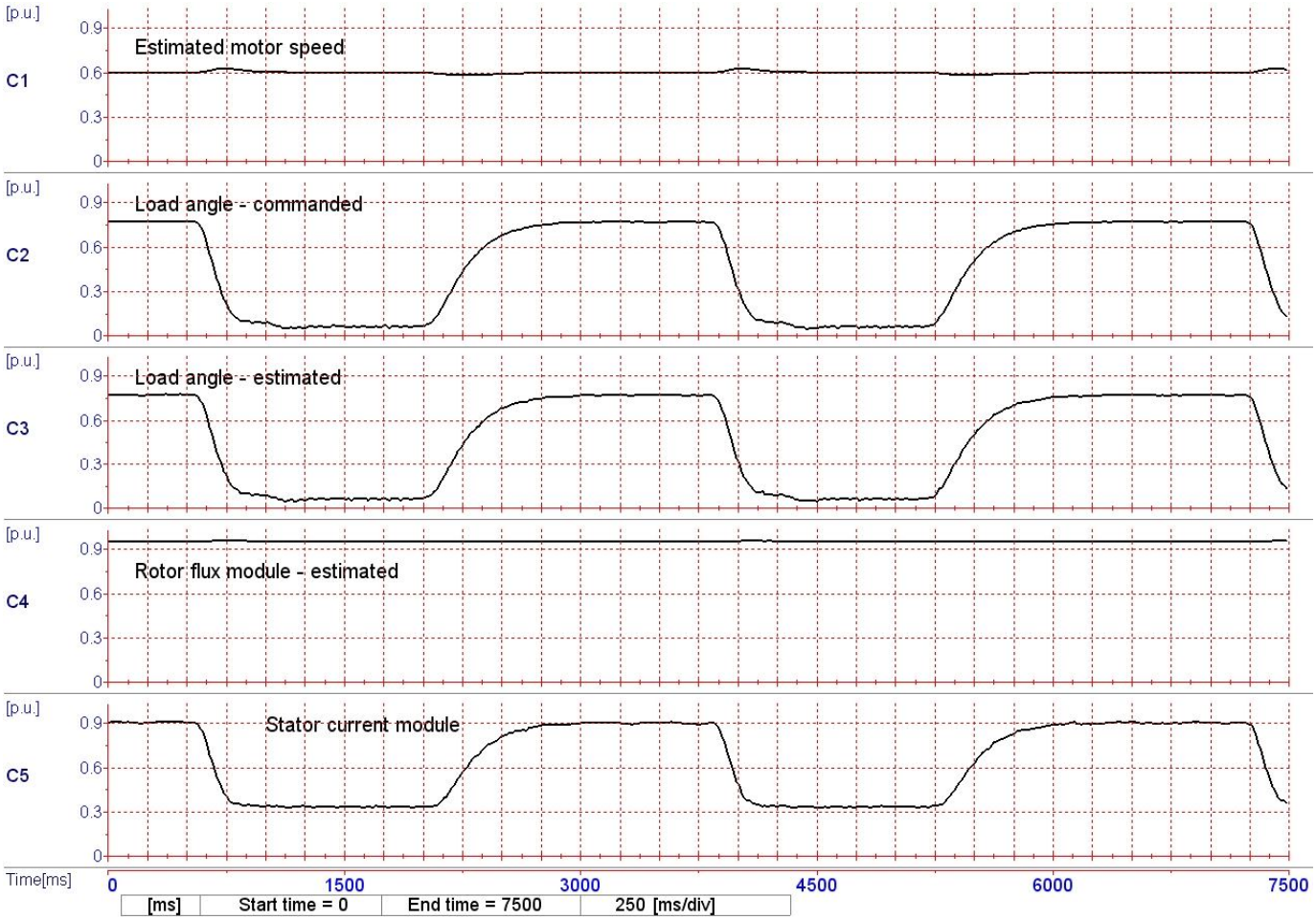

Fig. 19. The speed sensorless induction motor operation under load torque variation (Channels: C1- $\hat{\omega}_r$, C2-δ^{com}, C3- $\hat{\delta}$, C4- $\left|\hat{\Psi}\right|_r$, C5-$i_s$)

The load torque variations tests are presented in Fig. 19. Small speed variations are observed for moments of decreasing and increasing of the load. The speed error is compensated by an operation of PI controller.

VIII. CONCLUSIONS

In adjustable speed drives with induction motors and voltage inverters, the motor choke is sometimes installed to prevent overvoltages on the motor and inverter transistors. In the case of using sophisticated control of the motor, e.g. field oriented control without speed measurement, special attention should be taken to the motor choke.

Installation of the motor choke between an inverter and the motor introduces an unwanted voltage drop. Because of this drop, the motor voltage is not equal to the inverter output voltage. Unfortunately, the field oriented control algorithm is based on an assumption that a voltage generated by an inverter is equal to the motor supply voltage. This is the reason why some electric drives can not work correctly for such assumptions.

To solve this problem, some changes should be done in control and estimation algorithms as was presented in the paper.

Because field oriented control has inseparable coupling due to motor nonlinearities, good control properties of electric drives can be obtained with feedback linearization method. Such a method was implemented in the presented system.

Good properties of the proposed structure were confirmed by simulations and experimentally for 1.5kW speed sensorless drive.

THIS WORK WAS SUPPORTED IN PART BY THE SCIENCE FUND FOR THE YEARS 2008-2010 FOR THE FIRST AUTHOR. ADDITIONALLY, THIS PUBLICATION WAS MADE POSSIBLE BY AN NPRP GRANT FROM THE QATAR NATIONAL RESEARCH FUND (A MEMBER OF THE QATAR FOUNDATION). THE STATEMENTS MADE HEREIN ARE SOLELY THE RESPONSIBILITY OF THE AUTHORS.

APPENDIX

TABLE I. ASYNCHRONOUS MOTOR AND MOTOR CHOKE PARAMETERS

Asynchronous motor	
Power P_n	1.5 kW
Voltage U_n	400 V
Current I_n	3.5 A
Speed n_n	1410 rpm
Frequency f_n	50 Hz
Inertia J_M	0.0028 kgm^2
Stator resistance R_s	4.7 Ω
Rotor resistance R_r	4.76 Ω
Stator inductance L_s	0.32 H
Rotor inductance L_r	0.32 H
Mutual inductance L_m	0.3 H
Total leakage inductance $L_\sigma=L_s-L_m^2/L_r$	39 mH
Motor choke	
Inductance L_1	11 mH
Voltage drop in nominal load	5 %

TABLE II. DEFINITION OF THE PER UNIT VALUES

Definition	Description
$U_b = \sqrt{3}U_n$	base voltage
$I_b = \sqrt{3}I_n$	base current
$Z_b = U_b / I_b$	base impedance
$m_b = (U_b I_b p)/\omega_0$	base torque
$\Psi_b = U_b/\omega_0$	base flux
$\omega_b = \omega_0 / p$	base mechanical speed
$L_b = \Psi_b / I_b$	base inductance
$J_b = m_b/(\omega_b \omega_0)$	base inertia
$\tau = \omega_0 t$	relative time

REFERENCES

Bose B.K. (2009), "Power electronics and motor drives recent progress and perspective", *IEEE Transactions on Industrial Electronics*, Vol 56, No. 2, February 2009.

Vas P. (1990), *Vector Control of AC machines*, Clarendon Press, Oxford University Press, Oxford and New York.

Bogalecka E. (1992), : "Control system of an induction machine", EDPE 1992, High Tatras - Stara Lesna, Slovakia.

Isidori A. (1995), *Nonlinear control systems*, Springer-Verlag, London.

Krzemiński Z. (1987) "Non-linear control of induction motor", *10th IFAC World Congress on Automatic Control, Munich, Germany.*

Guziński J., Krzeminski Z., (2003), "Asynchronous motor nonlinear control with load angle controller use", *PES-4 Polish National Conference. 23-27 June 2003, Koscielisko, Poland.* (in Polish)

Kazmierkowski M.P., Malesani L., (1998) "Current control techniques for three-phase voltage-source PWM converters: a survey", *IEEE Trans on Industrial Electronics*, Vol. 45, No. 5, October 1998.

Abu-Rub H., Guzinski J., Krzeminski Z. (2004),"Advanced current regulated PWM inverter with simplified load model, *Electric Power Components and Systems*, Vol. 32, No. 10, October 2004.

Abu-Rub H., Guziński J., Krzemiński Z., Toliyat H. A. (2001), "Predictive current control of voltage source inverters", *The 27th Annual Conference of the IEEE Industrial Electronics Society. 29 November - 2 December 2001. Denver, Colorado, USA.*

Kouro S., Cortes P., Vargas R., Ammann U., Rodríguez J. (2009), "Model predictive control-a simple and powerful method to control power converters", *IEEE Transactions on Industrial Electronics*, Vol. 56, No. 6, June 2009.

Abu-Rub H., Guziński J., Rodriguez J., Kennel R., Cortés P. (2010), "Predictive current controller for sensorless induction motor drive", *IEEE International Conference on Industrial Electronics ICIT 2010, Vina del Mar – Valparaiso, Chile, 2010.*

Holtz J. (2006), "Sensorless control of induction machines—with or without signal injection?", *IEEE Transactions on Industrial Electronics*, Vol. 53, No. 1, February 2006, pp. 7- 30.

Krzemiński Z. (2000), "Sensorless control of the induction motor based on new observer", *Power Conversion and Intelligent Motion Conference PCIM 2000. Nürnberg, Germany, 2000.*

Binder A., Muetze A. (2008), "Scaling Effects of Inverter-Induced Bearing Currents in AC Machines", *IEEE Transactions on Industry Applications*, Vol. 44, No. 3, May/June 2008.
Akagi H., Hasegawa H., Doumoto T. (2004), "Passive EMI filter for use with a voltage-source PWM inverter having sinusoidal output voltage and zero common-mode", *IEEE Transactions on Power Electronics*, Vol. 19, No. 4, 2004.
Adamowicz M., J. Guziński J. (2005), "Control of sensorless electric drive with inverter output filter", *4th Int. Symposium on Automatic Control AUTSYM 2005. 22-23 September 2005. Wismar, Germany.*
Salomaki J., Luomi J. (2006), "Vector control of an induction motor fed by a PWM inverter with output LC filter", *EPE Journal*, Vol. 16, No 1, February 2006.
Wojciechowski D., Krzemiński Z. (2001), "Control System for the PWM Rectifier Based on Predictive Current Controller with Neural Network, *Power Conversion and Intelligent Motion Conference PCIM. Nürnberg, Germany, 2001.*
Guzinski J. (2008), "Closed loop control of ac drive with LC filter", *13th International Power Electronics and Motion Control Conference EPE-PEMC 2008. 1-3 September 2008, Poznan, Poland.*
Guzinski J. (2009), "Sensorless AC drive control with LC filter", *13th European Conference on Power Electronics and Applications EPE 2009. 8-10 September 2009r. Barcelona, Spain.*
Rajashekara K., Kawamura A., Matsuse K. (1996), *Sensorless control of ac motor drives*, IEEE Industrial Electronics Society. IEEE Press.
Krzemiński Z. (2008): Observer of induction motor speed based on exact disturbance model. International . *13th International Power Electronics and Motion Control Conference EPE-PEMC 2008. 1-3 September 2008, Poznan, Poland.*
Kubota H., Sato I., Tamura Y., Matsuse K., Ohta H., Hori Y. (2002), "Regenerating-mode low-speed operation of sensorless induction motor drive with adaptive observer", *IEEE Transactions on Industry Applications*, Vol. 38, No. 4, July/August 2002.
Chiasson J. (2005), *Modeling and High-Performance Control of Electric Machines*, IEEE Press and John Wiley Interscience, 2005.